J. Fluid Mech. (1974), *vol.* 63, *part* 2, *pp.* 209–224
Printed in Great Britain

Some properties of truncated turbulence signals in bounded shear flows

By ROBERT S. BRODKEY,
Department of Chemical Engineering, The Ohio State University, Columbus
JAMES M. WALLACE AND HELMUT ECKELMANN
Max-Planck-Institut für Strömungsforschung, Göttingen, West Germany

(Received 9 March 1973)

Earlier measurements of the contribution of four distinct classes of motions, i.e. ($u < 0, v > 0$), ($u > 0, v < 0$), ($u < 0, v < 0$) and ($u > 0, v > 0$), to the Reynolds stress $-\rho\overline{uv}$ in the wall region of a bounded turbulent shear flow have been extended. These classes were obtained by truncating the u and v signals about zero. Various statistical properties of the truncated streamwise and normal velocity components u and v and of their product uv have been determined in an attempt to characterize quantitatively the motions in this flow. Average values and probability density distributions both of the truncated and untruncated signals have been taken.

1. Introduction

In recent years there has been renewed interest in turbulent shear flows. This interest has been generated primarily by visual studies, notably those of Corino & Brodkey (1969) and of Kline and his co-workers, whose most recent published work is Kim, Kline & Reynolds (1971). These visual studies have shown that the fluid motions within such flows, far from being completely chaotic in nature, reveal a rather definite sequence of ordered motions. On the basis of these visual results, attempts have been made by several workers, using hot-wire and hot-film anemometry, to confirm the existence of these ordered motions and to obtain more quantitative information about them. A comprehensive review of studies of this region of the flow is given in Nychas, Hershey & Brodkey (1973). The studies most pertinent to our present work are reviewed briefly in this section.

Conditional averages taken by Blackwelder & Kaplan (1971) during the existence of such ordered motions, as indicated by their detection scheme, showed 'that during the burst there was a substantial streamwise momentum defect followed by an extremely rapid acceleration'.† They suggested that perhaps a

† At this point it seems appropriate to suggest a unifying terminology for the names of events. Kline *et al.* (1967) used the term 'burst' to describe the entire sequence of events consisting of lifting of low-speed fluid, oscillatory growth and breakup. We suggest retaining this term for the entire sequence. Corino & Brodkey described the sequence in terms of deceleration and a rapid outward motion called 'ejection' followed by a higher speed event.

local instability is the source of the breakup of the wall flow. Using a different detection scheme, Willmarth & Lu (1972) have shown that, during such motions, very large contributions to the Reynolds stress $-\rho\overline{uv}$ (sometimes as large as 62 $\overline{uv}$) can be measured. Laufer & Badri Narayanan (1971) have indicated that the frequency of occurrence of such structures, as seen by a stationary observer, is only dependent on the outer flow and length variables U_∞ and δ. In a more extensive investigation of this frequency, Rao, Narasimha & Badri Narayanan (1971) have also found that the frequency scales with the outer variables. Meek (1972), on the other hand, using more extensive data, claimed that inner variables u_τ and ν are the proper scaling parameters. Gupta, Laufer & Kaplan (1971) have investigated the lateral extent of such structures by using a short-time, cross-correlation technique. Their investigations showed that the lateral scale of the structures is about $100z^+$ units, which is in very good agreement with the visual results of Kline *et al.* The most recent visual results are those of Grass (1971). Using the hydrogen-bubble technique, he was able to obtain instantaneous values of the streamwise and normal velocity components over quite a large field in the wall region. His results confirm the existence of the motions in the wall region that had been observed by Kim *et al.* and Corino & Brodkey. He particularly emphasized the important contribution to the Reynolds stress of 'inrushes' of high-velocity fluid towards the wall.†

The present authors (1972) have measured, over the whole wall region, the contribution to the Reynolds stress of the four combinations of the truncated u and v signals, i.e. $(u < 0, v > 0)$, $(u > 0, v < 0)$, $(u < 0, v < 0)$ and $(u > 0, v > 0)$. The relationship between these four classes and visually observed events will be discussed later. In the work referred to above, Willmarth & Lu have made similar measurements at the single y^+ position of 30. Both studies show that the combined time-averaged contribution to the Reynolds stress of the higher momentum fluid moving towards the wall (sweep-type event) and the lower momentum fluid moving outwards from the wall (ejection-type event) is considerably in excess of 100 % of the stress over the whole wall region. This excess is reduced to 100 % by the two other combinations of the truncated u and v signals, i.e. lower momentum fluid moving towards the wall and higher momentum fluid moving away from the wall. We re-examined these latter motions using Corino's films and found them to be, in part, interactions between the motions giving the primary contribution to the Reynolds stress, i.e. ejections and sweeps. An estimate of the scales of these four categories showed that the sweep- and ejection-type motions were considerably larger than the interaction-type motions.

The investigations described above are indicative of the recent widespread interest in wall turbulent shear flows. Each research group is attempting to

† The 'inrushes' described by Grass (1971) correspond to the term 'sweep' introduced by Corino & Brodkey. It is suggested that the latter be used for describing accelerated motions towards the wall. Nychas *et al.* restricted the term sweep to the nearly parallel flow near the wall, while using the term 'high-speed event' for the entire accelerated flow that extended from the wall to the outer flow. There seems to be no real advantage in separating these two, although it should be recognized that the angle of flow towards the wall decreases as the wall is approached.

study the characteristic motions in this wall region, which must, necessarily, be the same in each of these similar flows; the methods used, however, are different. It is impossible to say, *a priori*, that the motions detected by the different schemes are identical because the criterion used in each case is different. Only *a posteriori* can it be inferred from the results whether the motions detected were indeed similar. For example, Blackwelder & Kaplan used a detection scheme based on the magnitude of the variance of the u signal about a short-time average. They measured short-time average u velocities as functions of time and normal position. Willmarth & Lu, in addition to the measurements in the four quadrants described above, used an event detection criterion based on the amplitude and slope of the u signal. They reported short-time averaged uv measurements as functions of time as well as other statistics of the detected signals. Rao *et al.* used the time derivative of u as a detection signal, which was then discriminated, and measured only the frequency of flow events. The visual studies were easier to interpret physically, but the statistical quantities that could be obtained from them were limited and suffer from the relatively small sample sizes. Where possible, the quantities measured and reported here will be compared with similar results measured by others. In this manner it can, we hope, be established whether the various methods are detecting similar events.

Our investigation is based primarily on the visual study of Corino & Brodkey, which has been supported by and supports the visual results of others. At the risk of being repetitious for readers who are familiar with this picture, a brief description of the sequence of motions that Corino & Brodkey observed visually will be given again since it is essential for the interpretation of the present results.†

The sequence began with a local deceleration of the flow over a rather large region near the wall. The flow within this decelerated region had very small velocity gradients, so that it flowed almost as a plug; at its edges, however, there existed extremely high velocity gradients, giving rise to high shear rates. From within this decelerated region, there occurred suddenly an ejection of fluid outward from the wall with a large normal velocity component. This was observed by Corino & Brodkey to be the most important event in the wall region. Following these ejections there appeared a mass of fluid with dimensions larger than the ejection scale, which moved with velocities greater than the mean and nearly parallel to or at a slight angle towards the wall (sweep). These events were observed to occur randomly in space and time but approximately in this sequence. As mentioned earlier, a re-examination of these films by the present authors indicated that between these two larger scale motions, which make very large contributions to the Reynolds stress, there often occurred an interaction in which occasionally the low-speed ejecting fluid was deflected back towards the wall and the incoming, accelerated, fluid was reflected outwards from the wall. These interaction-type motions give rise to negative instantaneous contributions to the Reynolds stress. We have attempted in our earlier work to confirm the

† An attempt has been made by Nychas *et al.* to give a composite picture of the flow in the entire wall and outer regions. A complete picture must, however, wait for three-dimensional experimental results, both visual and from anemometry.

existence of this sequence and to investigate in more detail some of its properties. The present work is an extension of the earlier with much more detailed and complete measurements.

2. Experimental facility and data acquisition

The flow facility used for this investigation is the oil channel used by the authors in the previously cited work. At this point, we need only describe the main features of the channel and flow. The flow is turbulent, tripped at the beginning of the entrance length, and fully developed; the channel is 22 cm wide and 85 cm deep with an 8 m long entrance length. It is fitted with a top cover. The measurements were made halfway between the top and the bottom of the channel, which is outside the boundary layers on both surfaces. All the data reported here were taken for a constant flow rate in the channel, with a centre-line velocity of 21 cm/s. The shear velocity u_τ was 1·06 cm/s, and the kinematic viscosity of the oil used in the channel was 0·06 cm^2/s. The Reynolds number based on the centre-line velocity and the channel width was 7700. An estimate of the equivalent Reynolds number, based on the momentum thickness for a boundary layer assuming a $\frac{1}{7}$-power law, yielded about 430. As was pointed out in our previous work, this channel was designed to give a very large viscous sublayer. In the channel, 1 cm is equivalent to $y^+ \approx 18$, and it was possible to position an X-probe as close as $y^+ \approx 3{\cdot}5$. The centre-line of the channel corresponds to $y^+ = 195$. A Thermo-Systems, Inc. X-probe, type 1241-20W, was used, and the constant-temperature anemometer and linearizer used were also made by them. The smallest event in the Corino & Brodkey visual study was of the order of $30x^+$ units in the flow direction and of at least $30y^+$ units in the normal direction. The probe used here had sensing lengths less than $2x^+$ and $2y^+$ units.

To obtain the u and v signals to be digitized and analysed, the linearized output voltages of the two films of the X-probe were manually balanced as carefully as possible and then digitized and stored on a magnetic disk. The digitizing rate, based on the Nyquist frequency criteria, was 50 samples/s. To obtain adequate statistical samples, very long run times were necessary because of the nature of the flow system. In this case, 45 min sampling times were used for each y^+ position. The analysis of the digitized data was done with a computer program developed by the authors instead of the previously used analog techniques. To obtain the streamwise and normal fluctuating velocity component signals u and v for analysis, the manually balanced output voltages of the anemometers were exactly balanced with an iteration loop in the program, using the criterion that the time average $\overline{V}$ of the velocity component normal to the wall must equal zero. The balanced signals were subsequently added and subtracted to obtain u and v. A PDP-15 computer, made by Digital Equipment Corporation, was used for all the analysis in this work. The critical question, which arises in all experiments of this type, of the error introduced by the w fluctuations has been considered in Eckelmann (1974). In addition, the question of the sensitivity to temperature is also considered there. He has concluded that the errors introduced by w fluctuations are less than 5 % and that temperature fluctuations are negligibly small.

Sign of u	Sign of v	Sign of uv	Type of motion
−	+	−	Ejection
+	−	−	Sweep
−	−	+	Interaction (wallward)
+	+	+	Interaction (outward)

TABLE 1

3. Experimental results

The primary result of our previous work was the measurement of the contribution to the Reynolds stress in the wall region of the four types of motion tabulated in table 1. Also tabulated are the visually observed events that can be associated with these four types of motions. In the remainder of this paper the terms, descriptive of visually observed motions, in the last column of table 1 will be used to indicate the four categories of motions with the signs shown in the table. This is for convenience, and it should be understood that there does not exist a one-to-one correspondence between the visually observed motions and the four categories of the truncated u and v signals. The categories of the truncated signals must, however, include most of those corresponding visually observed motions because of the correspondence of the signs of the velocity components u and v in the two types of investigation. The data from our previous work, which had been stored on analog tape, was originally analysed by analog methods. As a preliminary to this study, these data were digitized and reanalysed by digital methods. The contributions to the Reynolds stress, $-\rho\overline{uv}_c/-\rho\overline{uv}$, where $-\rho\overline{uv}_c$ is the time-averaged Reynolds stress of each class, were again determined, and the previous results were exactly confirmed, giving us confidence in this new digital analysis procedure. The new data were directly digitized, stored on the computer disk and subsequently analysed digitally. The results plotted in figure 1 show the same trends as our previous results obtained by analog methods, but the values in all four categories are somewhat greater than those measured earlier. This was apparently due to a property of the tape recorder discovered later. We recorded the data at a very low tape speed, but played it back for analysis at 100 times the speed at which it was recorded. At this faster playback speed, the amplitudes were reduced by 13%. This effect could very well account for the differences in the two sets of results. As observed earlier, the plot shows clearly that four distinct types of motion which have different contributions to the Reynolds stress exist in the wall region. As mentioned in the introduction, Willmarth & Lu had made the same measurements at the single y^+ position of 30, independently. Their results are also shown in the plot and are seen to be similar. The contribution of the ejection-type motion is greater than that of the sweep-type motion for $y^+ \gtrsim 15$, and both are larger than the contributions to the Reynolds stress of the interaction-type motions. The difference in the magnitude of their values and ours have been attributed by Willmarth & Lu

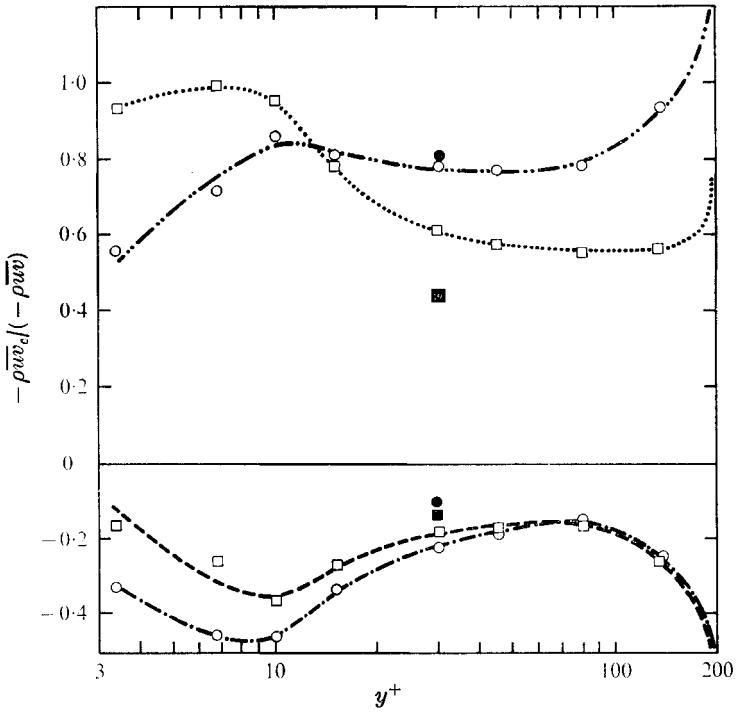

FIGURE 1. The classified Reynolds stresses normalized with the local average Reynolds stress. ●, ■, results of Willmarth & Lu (1972). ·····, sweep; —·—, ejection; —·—, i_o, outward interaction; – – –, i_w, wallward interaction.

to a possible Reynolds number effect which we hope to investigate in the near future.†

Figure 2 shows the same term, $\overline{uv}_c$, normalized with u_τ^2. In contrast to figure 1, this is a plot of the absolute contribution to the total Reynolds stress of the four classes of motions at each y^+ position, whereas figure 1 showed the fractional contribution to the local total Reynolds stress. Normally, this term is plotted linearly against y^+, but here we have plotted it logarithmically to emphasize the wall region. It is seen that the maxima of all four categories occur in the region $20 \lesssim y^+ \lesssim 40$. Both figures 1 and 2 show that ejection-type motion contributes about 25% more to the total Reynolds stress than sweep-type motion in this region.

It will be useful, at this point, to define (see figure 3) a number of 'average time' quantities which have been measured to characterize further the events in the flow. These are an average duration of the events, an average period between events and the fraction of the total time that the signal is in the respective categories. This latter is sometimes called the duty cycle.

Considering first the fraction of time that the flow passing the probe is in each category (duty cycle), as shown in figure 4, it is seen that the ejection events occupy about 20% less time than the sweep events in this same region of $20 \lesssim$

† After this paper was submitted for publication, further results were reported by Lu & Willmarth (1973) which show a different trend for lower y^+ values.

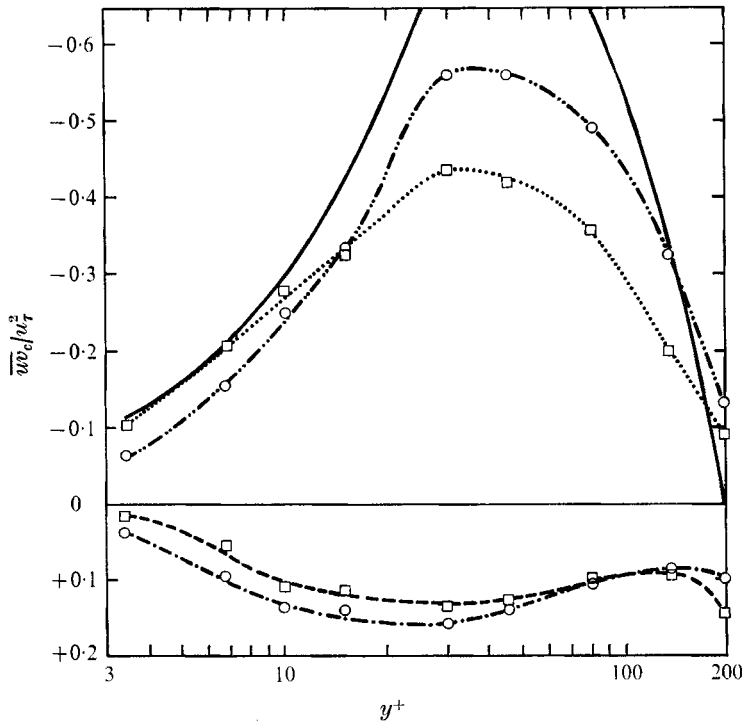

FIGURE 2. The classified Reynolds stresses normalized with the friction velocity squared. ·····, sweep; —·—, ejection; —·—, i_o; – – –, i_w; ——, total.

FIGURE 3. Illustration of 'average time' quantities measured.

$y^+ \lesssim 40$. In other words, the ejection-type motions on the average contribute 25% more to the Reynolds stress in about 20% less time than do sweep-type motions. In the region very near the wall, the opposite is seen to be true. From figure 4 one also sees that the percentage of time spent in the categories varies little over the whole measurement range for all four categories. Kim *et al.*

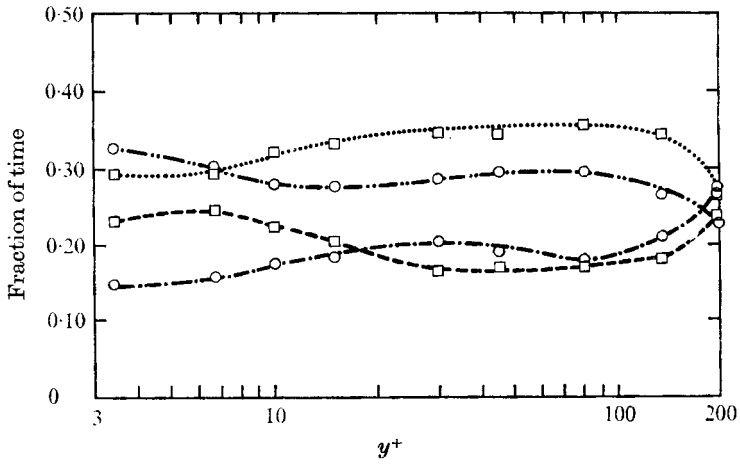

FIGURE 4. Fraction of time the signals are in the respective categories. ·····, sweep; —·—·—, ejection; —·—·—, i_o; – – –, i_w.

measured the fraction of the total time occupied by bursts. They indicated that the instantaneous Reynolds stress was almost always positive during these periods. Thus these periods should correspond approximately to the sum of the ejection and sweep periods. From our figure 4 one sees that this sum is nearly constant at about 0·61, which compares extremely well with their reported value of 0·55 in the region $y^+ < 30$ (their figure 13). Measurements by the hydrogen-bubble method beyond this position are progressively less sensitive to the sweep motions so that one would expect the values reported by Kim *et al.* to decrease to the level given by ejection motions alone. From our figure 4, this value is 0·28 for $y^+ > 30$, and in their figure 13, the curve decreases to a value of 0·30. The agreement is excellent and our results, which separate the ejection and sweep contributions, provide further insight into the nature of the variation with y^+ that they reported.

The consequences of figures 2 and 4 are seen in figure 5. Here the classified $\overline{uv}$ values, normalized with u_τ^2 (as in figure 2), are divided by the fraction of time spent in the categories of figure 4 to yield the average, normalized, classified $\overline{uv}$ values of an average event. This is equivalent to averaging the uv signal only when the flow passing the probe is in a particular category and then normalizing with u_τ^2. Figure 5 shows that an ejection-type motion on the average is approximately $\frac{1}{3}$ larger than a sweep-type motion at $y^+ = 30$. This is a result of both the higher contribution of ejection-type motions and the lower fraction of the time for which they exist.

In the construction of figure 5, the fraction of the total time spent in the various categories was used, but not information about their average (time) duration or about the average period between occurrences. It contains only information about the magnitude of the average uv values of average events. Figure 6 shows the average duration of such average events over the measurement range of this study. Both dimensional and non-dimensional forms (in terms of outer variables) of this quantity are given. It is interesting to observe that although the two

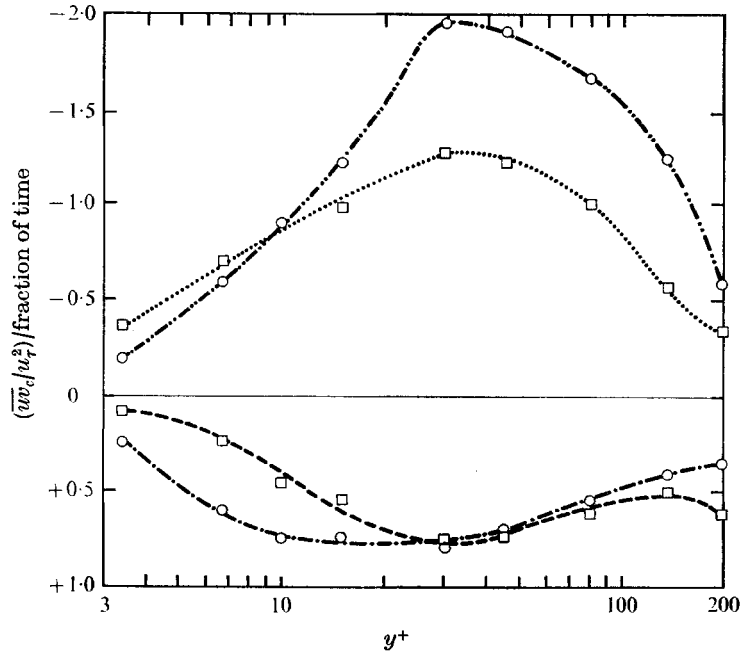

FIGURE 5. The classified Reynolds stresses divided by the fraction of time in the respective classes. Equivalent to time averaging with the sum of the event durations. Notation as in figure 4.

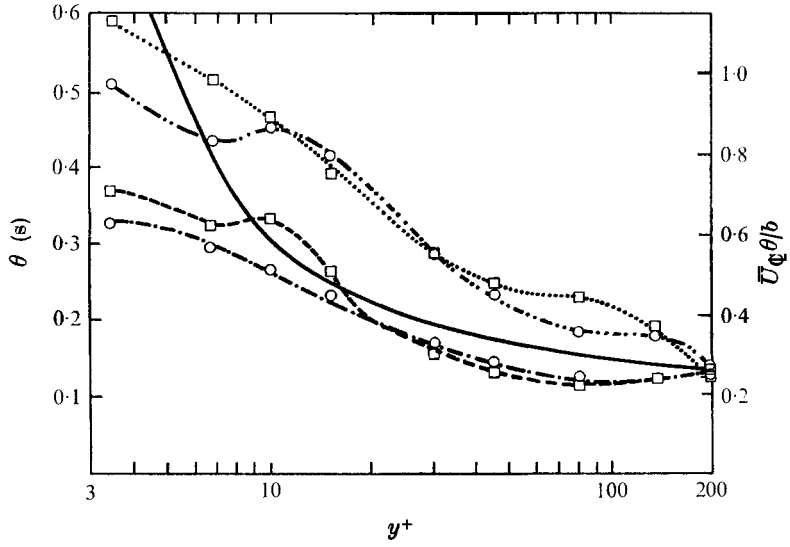

FIGURE 6. The average duration of events. Notation as in figure 4.

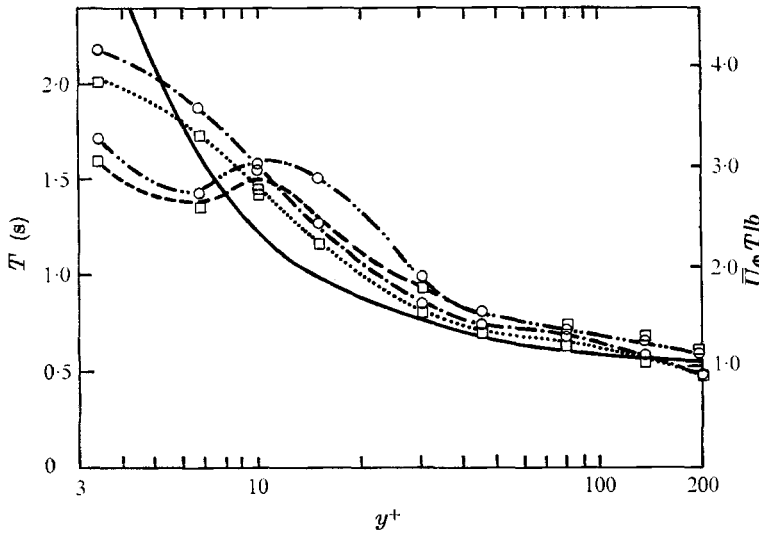

FIGURE 7. The average period between events. Notation as in figure 4.

positive contributors to the Reynolds stress, i.e. ejection- and sweep-type motions, show considerably longer average durations than the two interaction-type motions, in agreement with our previous autocorrelation measurements (see Wallace *et al.* 1972), the shapes of the curves show pairings of ejection-type motions with wallward-interaction-type motions and sweep-type motions with outward-interaction-type motions. These pairings have in common the sign of their streamwise velocity components u. The ejection-type and wallward-interaction-type motions are regions of decelerated fluid and the sweep-type and outward-interaction-type motions are regions of accelerated fluid. The same pairings of the categories are more clearly seen in figure 7, where the average period between occurrences of the various categories is plotted as a function of y^+, again in both dimensional and non-dimensional form. The smaller period as well as the shorter duration with increasing distance from the wall is, in part, a reflexion of the increasing mean velocity. This is shown in figures 6 and 7 by the solid lines calculated by simply multiplying the centre-line value by the ratio of the centre-line velocity to the mean local velocities. Outer variables were used in normalizing time terms, since, as will be noted shortly, these are apparetly the appropriate scaling parameters to obtain invariance with Reynolds number. This does not mean that the period (and the duration) will not vary across the flow field. As may be seen in the figures, they do vary considerably in the near-wall region. Rao *et al.* obtained similar results for the outer region only ($y^+ \geqslant 30$). The variation of the period they observed in this region is similar to ours; however, exact comparison is not possible because of the unknown effect of intermittency on the period in a boundary layer. Our experiments were in a fully developed channel flow and thus with no intermittency.

If the maximum period of ejection-type motions in the range of their major occurrence ($10 < y^+ < 45$) is taken as representative of the event period, it can be compared with the period measurements of others. For this low Reynolds number

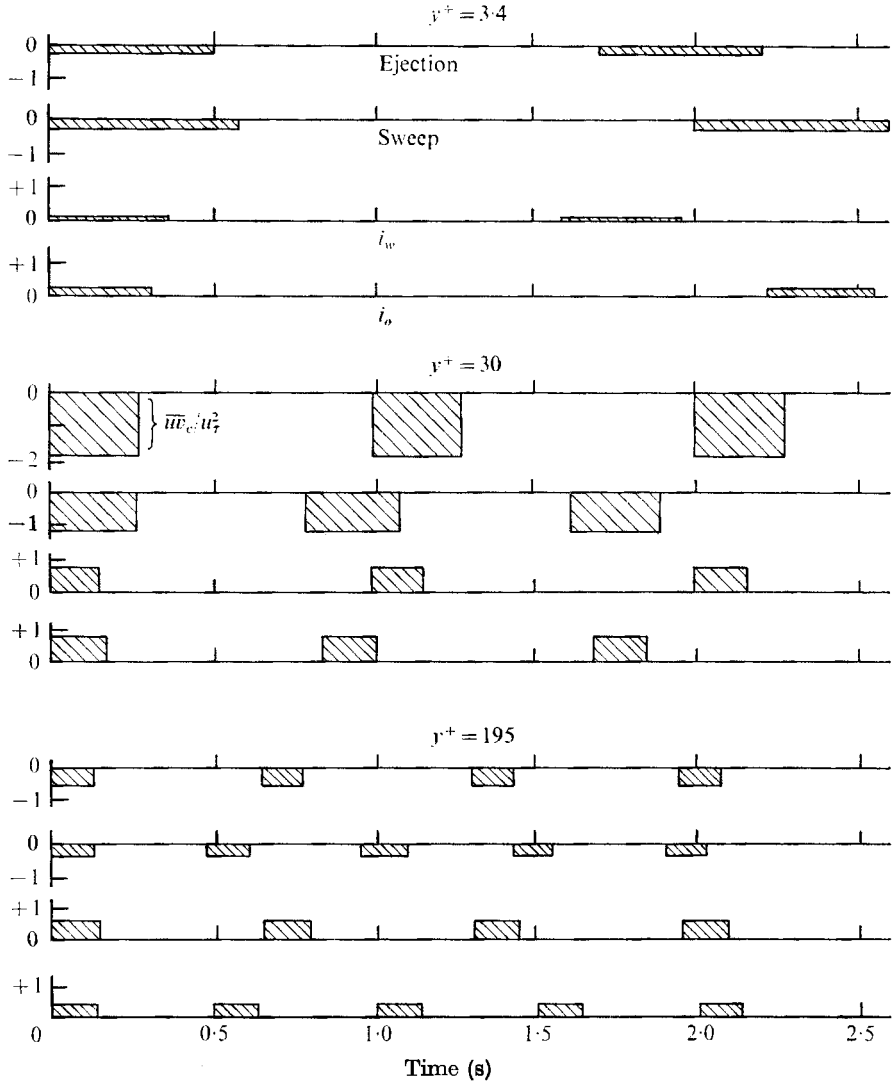

FIGURE 8. Illustration of average event durations, period between events and amplitude of uv signals during events.

experiment ($Re \approx 430$), the non-dimensional period, where b is the channel half-width, is

$$T^* = \bar{U}_{\mathbb{C}} T/b = 3{\cdot}0 \quad \text{or} \quad T^+ = u_0^2 T/\nu = 26.$$

These values agree reasonably well with the curves presented by Laufer & Badri Narayanan. They agree almost exactly with the curve of Rao *et al.* Their value was obtained by a discriminator level technique; our technique is similar to theirs in that, for example, the ejection quadrant is a discriminator with zero discrimination level. Our work thus supports the use of outer variables for scaling. It disagrees with the conclusions of Meek. It should be noted that Meek misused the data of Corino & Brodkey by presuming that the number of disturbances was

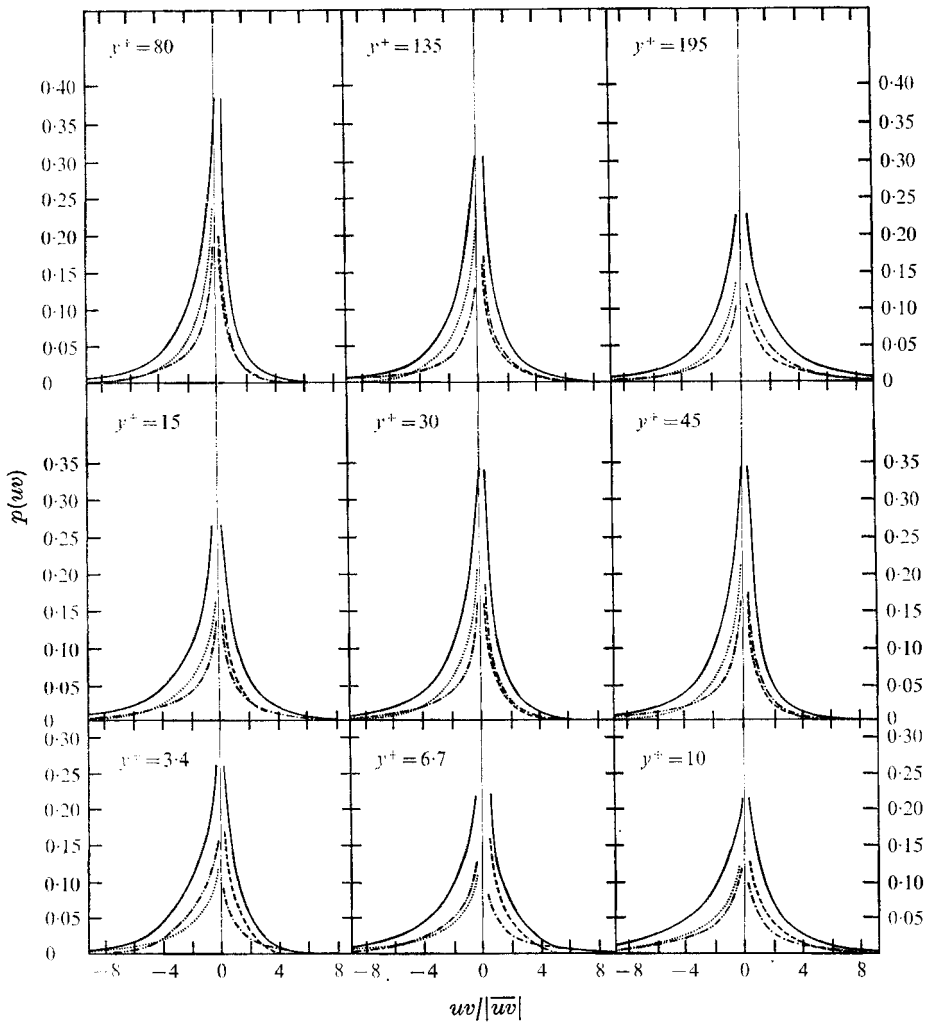

FIGURE 9. The probability density distribution of uv. Notation as in figure 2.

observed at a point on the wall rather than in a moving frame of reference. Thus his estimate of $\sqrt{T^+} = 15$ for this data is too high and, if reduced, would also agree better with the above-mentioned works.

From figures 5–7, one can construct idealized classified uv signals where the amplitude, length and period between events are values averaged only within each category. Such idealized classified uv signals for three y^+ positions across the channel half-width are shown in figure 8. This figure should not be misinterpreted. These plots are components of idealized uv signals with amplitudes lengths and periods between events made equal to the average values of these properties of the real signals. The real signal is not, of course, uniformly spaced and of uniform height and width, nor is it rectangular. Figure 8 does, however, summarize the average characteristics of the four categories of motions.

The degree of deviation of the instantaneous uv magnitudes about the averages

is clearly seen in figure 9, where the probability density of the uv signal, unclassified and classified into the four categories, is plotted against uv normalized with the absolute value $|\overline{uv}|$ of the local average. In the case of the centre-line, the normalization factor $|\overline{uv}|$ is zero, so a ratioed scaling factor (obtained from the ratio of $p(uv)$ at $y^+ = 195$ and 135 calculated with unnormalized uv abcissa intervals) was used in order to scale the distribution at this position for comparison with the other results. In figure 9 the sums of the classified probability densities for a particular $uv/|\overline{uv}|$ equals the probability density of the unclassified signal at that value. Thus

$$\int_{-\infty}^{+\infty} p(uv)\, d\left(\frac{uv}{|\overline{uv}|}\right) = \int_{-\infty}^{+\infty} [p_{ej}(uv) + p_{sw}(uv) + p_{iw}(uv) + p_{io}(uv)]\, d\left(\frac{uv}{|\overline{uv}|}\right) = 1,$$

where the subscripts indicate the categories. The average values of the classified conditions, which were plotted in figure 1, are given by

$$\frac{-\rho\overline{uv}_c}{-\rho\overline{uv}} = -\int_{-\infty}^{+\infty} \frac{uv}{|\overline{uv}|}\, p_c(uv)\, d\left(\frac{uv}{|\overline{uv}|}\right).$$

In general, for equal areas under the distribution curves, a larger flatness factor results in larger values of $-\rho\overline{uv}_c/-\rho\overline{uv}$ because of the greater contribution to the averages from the large values at the tails of the curves. The basic shapes of the unclassified curves, i.e. their large peaks at $uv = 0$ and long tails, agree well with similar curves reported by Willmarth & Lu and by Gupta & Kaplan (1972). The new information provided here is the classified distributions. From these it is seen that the sweep and outward-interaction curves have larger flatness factors than the other two categories in the wall region, and the ejection and wallward-interaction curves have larger flatness factors nearer the channel centre in agreement with figure 1. It can also be seen that, for $y^+ > 30$, essentially all the very large instantaneous uv values ($uv > 8\overline{uv}$) lie in the ejection category. Very close to the wall ($y^+ = 3{\cdot}4$) these very large uv pulses come from the sweep motions alone. This is in good agreement with the visual observations of Corino & Brodkey, who saw that the ejections originated slightly away from the wall ($5 < y^+ < 30$), but that the sweep motions could come all the way to the wall. The wallward-interaction distribution curves change with y^+ in a similar manner to those of the ejection motions; the outward-interaction and sweep distributions are likewise similar. This again shows the dominant role played by the common sign of the streamwise velocity component in these pairs of categories as was seen earlier in figures 6 and 7.

The probability density distributions of the u and v velocity components themselves give further insight into the characteristics of the motions giving rise to these Reynolds stresses. Figures 10 and 11 show the probability density distributions $p(u)$ and $p(v)$ of the u and v signals plotted against u and v normalized with the local mean velocity $\overline{U}$ for nine positions across the channel half-width. The solid curves in the two plots are the distributions of the unclassified u and v values respectively. These are in good agreement with similar results of Eckelmann (1974) and of Gupta & Kaplan (1972). The other four curves in each plot

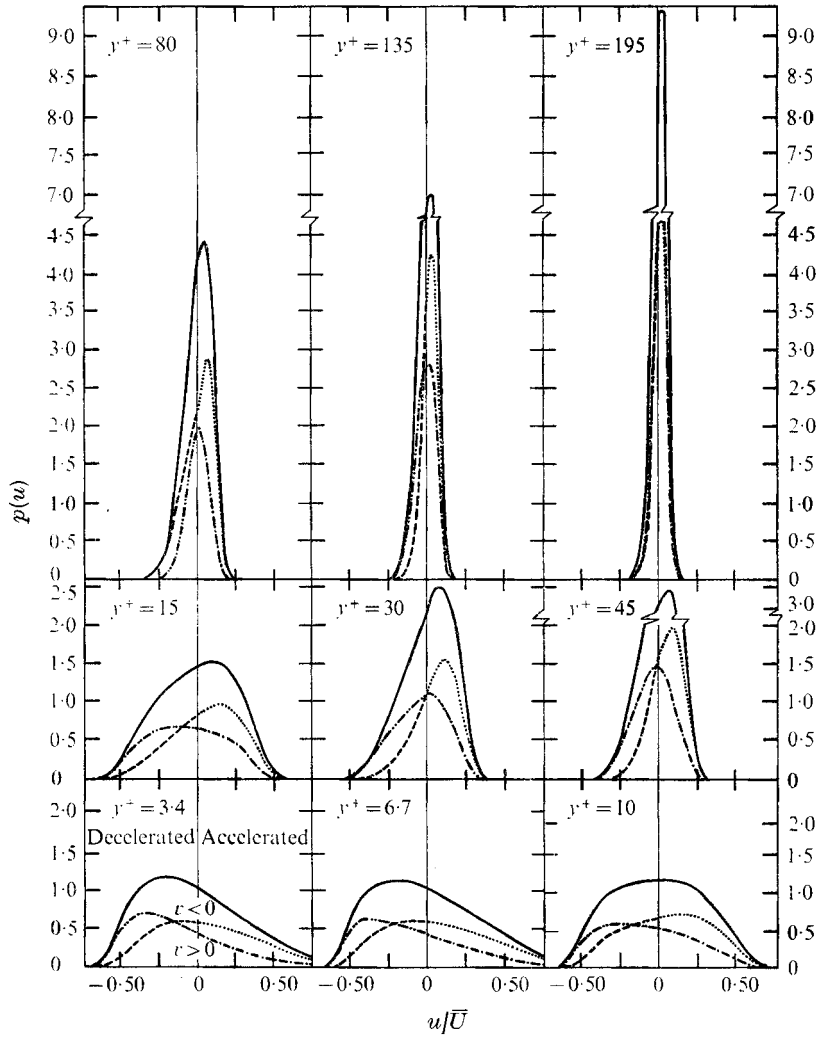

FIGURE 10. The probability density distribution of u. Notation as in figure 2.

are the distributions of the values in the four categories. The four classified distributions in each plot form two continuous curves. The sums of these are equal to the unclassified distributions, and thus the latter can be pictured as a combination of two distributions which are more easily interpreted. In figure 10 the two curves represent the u distribution for flow away from the wall ($v > 0$; ejection motions and outward-interaction motions) and for flow towards the wall ($v < 0$; sweep motions and wallward-interaction motions). In figure 11 these represent the v distributions for flow moving at less than the local mean streamwise velocity ($U < \overline{U}$ or $u < 0$; ejection motions and wallward-interaction motions) and flow moving at greater than the local mean ($U > \overline{U}$ or $u > 0$; sweep motions and outward-interaction motions).

Considering these two figures, it is seen that the decelerated flow of figure 11 shows a fairly strong tendency to move predominantly away from the wall at

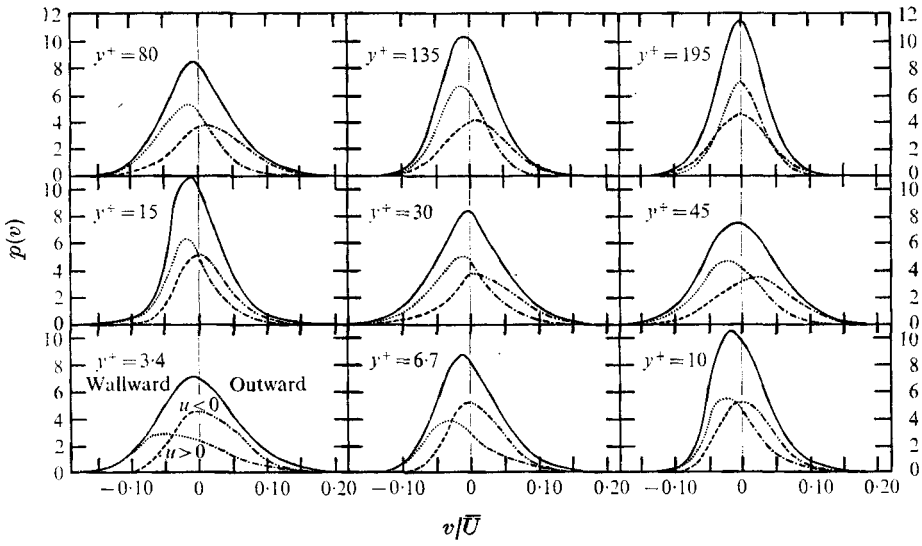

FIGURE 11. The probability density distribution of v. Notation as in figure 2.

y^+ positions of 30 and 45. Since this decelerated flow (left-hand side of figure 10) lies mainly in the ejection category at these positions, as well as over the rest of the channel half-width, this accounts for the dominance of the ejection category in this region, as observed in figures 2 and 5. This is the region where a concentration of ejection events would be expected from the results of visual studies. The curve representing accelerated flow in figure 11, on the other hand, is seen to lie mainly on the negative side of the ordinate, indicating accelerated flow towards the wall. This is generally true over the entire channel half-width but not as pronounced as for the decelerated fluid at $y^+ = 30$ and 45. This accounts for the flatter shapes of the sweep curves in figures 2 and 5. Visual studies have also indicated that the sweep motions are larger scale and thus less concentrated in a narrow y^+ range. Near the wall, in the region where highly decelerated 'plug' flow is known to occur, figure 10 shows that the most probable velocities are highly decelerated. The most probable u velocity at $y^+ = 6{\cdot}7$ for example, with $v > 0$, is 40 % less than the local mean.

There is a close consistency between these results and the conclusions of Grass based on conditionally averaged instantaneous velocity profiles. He found that minimum local u velocities correspond closely to maximum outward v velocities, especially in the region beyond $y^+ = 25$. Also, maximum local u velocities were seen to correspond closely to maximum inward v velocities. For his smooth-wall study, the correspondence is particularly strong in the regions $25 < y^+ < 80$ and $120 < y^+ < 170$. It is not clear why the correspondence is not seen in the region $80 < y^+ < 120$. We do not see this change in our figure 11; however, one should note that our distributions for the sweep in this region involve 35 % of the total sample, which is quite large. The conditionally averaged profiles of Grass involve just 12 of his instantaneous profiles, which may not be enough. This could account for the discrepancy.

4. Summary

The four categories into which the u, v and product, uv, signals have been divided apparently do contain the types of motion observed visually in the films of Corino & Brodkey. Although additional, extraneous motions are undoubtedly also included in these categories, it is believed that the dominant features of their properties reflect the nature of ejections, sweeps, and wallward and outward interactions. Thus we conclude that ejections and sweeps are, on the average, considerably more intense and of a larger scale than the interaction-type motions. All four occur with about the same frequency for $y^+ > 10$. Ejection-type motions have been shown to be about $\frac{1}{3}$ more intense than sweep-type motions in the region of maximum Reynolds stress, because they have both larger average stresses and exist for 20 % less of the time.

Probability density distributions of the truncated signals provided details of the composition of the categorized events.

The authors would like to thank Dr John Heibel and Herr Paul Habermann for much valuable help in developing the computer program used in this work. Thanks are also due to Frl. P.-D. Pfufzen for her computational help. One of us (R.S.B.) received support from a NATO Senior Fellowship in science as well as help from the MPI during part of this joint effort. This paper is part 1 of a paper presented at the 13th IUTAM Congress held in Moscow in August 1972.

REFERENCES

Blackwelder, R. F. & Kaplan, R. E. 1971 *AGARD Conf. Proc.* no. 93.

Corino, E. R. & Brodkey, R. S. 1969 *J. Fluid Mech.* **37**, 1.

Eckelmann, H. 1974 Submitted for publication in *J. Fluid Mech.*

Grass, A. J. 1971 *J. Fluid Mech.* **50**, 233.

Gupta, A. K. & Kaplan, R. E. 1972 *Phys. Fluids*, **15**, 981.

Gupta, A. K., Laufer, J. & Kaplan, R. E. 1971 *J. Fluid Mech.* **50**, 493.

Kim, H. T., Kline, S. J. & Reynolds, W. C. 1971 *J. Fluid Mech.* **50**, 133.

Kline, S. J., Reynolds, W. C., Schraub, F. A. & Runstadler, P. W. 1967 *J. Fluid Mech.* **30**, 741.

Laufer, J. & Badri Narayanan, M. A. 1971 *Phys. Fluids*, **14**, 182.

Lu, S. S. & Willmarth, W. W. 1973 *J. Fluid Mech.* **60**, 481.

Meek, R. L. 1972 *A.I.Ch.E. J.* **18**, 854.

Nychas, S. G., Hershey, H. C. & Brodkey, R. S. 1973 *J. Fluid Mech.* **61**, 513.

Rao, K. N., Narasimha, R. & Badri Narayanan, M. A. 1971 *J. Fluid Mech.* **48**, 339.

Wallace, J. M., Eckelmann, H. & Brodkey, R. S. 1972 *J. Fluid Mech.* **54**, 39.

Willmarth, W. W. & Lu, S. S. 1972 *J. Fluid Mech.* **55**, 65.